The magnetic field dependence of shallow donor impurity states in GaAs/GaAlAs multi-quantum wells: a non-variational approach

1994 J. Phys.: Condens. Matter 6 757

(http://iopscience.iop.org/0953-8984/6/3/016)

J. Phys.: Condens. Matter 6 (1994) 757–770. Printed in the UK

The magnetic field dependence of shallow donor impurity states in GaAs/GaAlAs multi-quantum wells: a non-variational approach

T Kuhn†, G Mahler†, J L Dunn‡ and C A Bates‡

† Institut für Theoretische Physik, Universität Stuttgart, Pfaffenwaldring 57, 70550 Stuttgart, Federal Republic of Germany

‡ Physics Department, The University, Nottingham NG7 2RD, UK

Received 6 October 1993

Abstract. We present a novel approach to the calculation of shallow impurity states in single- and multi-quantum-well systems. The Schrödinger equation is directly integrated numerically using an iterative technique. Thus, by avoiding a variational *ansatz* for the wave function and including a proper treatment of the coupling between the wells, the whole range from low to high magnetic fields as well as from the two-dimensional to the three-dimensional limit is treated on the same level. For the case of a single quantum well we discuss the dependence of the binding energies on the magnetic field as well as on the position of the impurity. For the case of a multi-quantum-well system we analyse the influence of the barrier width on the energies and the localization of the wave functions and we show that for barriers thicker than about 10 nm a single-well analysis is sufficient. A comparison with experimental results shows good agreement.

1. Introduction

The study of shallow impurities in the presence of a magnetic field is of considerable interest experimentally because of their effect on the properties of device materials. For example, we note that resonant tunnelling of electrons through bound impurity states has recently been reported [1]. This follows earlier work [2] in which such impurities were shown to give rise to specific features in the current–voltage characteristics of double-barrier resonant structures via donor-assisted tunnelling. Such structures also provide an interesting theoretical subject for the investigation of the interplay between different length and energy scales. Characteristic length scales are given by the well and barrier widths, by the Bohr radius of the impurity, and by the cyclotron radius. Corresponding energy scales are given by the barrier height, the miniband width and splitting, the Rydberg energy of the impurity, and the cyclotron energy.

The problem has been studied extensively mainly using different variational approaches [3–7] as summarized, for example, for bulk materials in [8]. A variational approach is particularly useful if the characteristic lengths and energy scales are well separated as there is then a clear physical motivation for the selection of a trial wave function. In further work [9], an alternative matrix diagonalization procedure has been developed in order to calculate accurately the energies of all states and, in particular, those of the excited states. For low magnetic fields, hydrogen-like states will be slightly modified by the field, while for high fields Landau states will be slightly modified by the impurity. Also, if the well is

0953-8984/94/030757+14$07.50

thin compared to the Bohr radius, two-dimensional hydrogen-like states will be a good basis set, while in the opposite limit three-dimensional states should be taken. In a multi-quantum well system, the ratio of the binding energy to the miniband width strongly influences the localization of the states. If this ratio is large, the impurity states will be mainly localized inside one well; otherwise, they will be delocalized over several wells. Consequently, either localized or delocalized trial wave functions should be used.

The physically more interesting regime, however, is the case where two or more scales are of the same order of magnitude. Then, within a variational technique either a large number of variational parameters or some interpolation scheme such as two-point Padé approximations [10] have to be used. A neccessary condition for such an interpolation is the possibility to trace back each single state towards the two limiting cases. Obviously, this is not always possible. The absence of a one-to-one correspondence between low- and high-field states can lead to so-called metastable states [11–13] which cannot be obtained starting from the low-field limit.

The drawbacks of a variational approach can be avoided by a direct numerical solution of the time-independent Schrödinger equation. The numerical error resulting from the discretization of the differential equation can easily be controlled by using different sizes for the steps. Without a change in the basis set, the full parameter range can be investigated. In contrast to a variational or perturbational approach, the case of largely differing relevant scales would provide difficulties. For the present case, however, this does not happen. At low fields, the magnetic length scale is much larger than the Bohr radius, but this length is irrelevant for the wave functions. In the high-field limit the spatial extension of the states is determined by the cyclotron radius only while the Bohr radius is irrelevant. Thus, even if the problem is characterized by two different length scales, the solution has only one characteristic length.

The aim is to describe this novel approach to the calculation of the energies of impurity states in single- and multi-quantum-well systems. The paper is organised as follows. In section 2 the basic ideas of the technique for the solution, the theoretical model, and the details of the numerical method are described. In the following sections 3 and 4, we present our results for the single-quantum well (SQW) and multi-quantum-well (MQW) systems, respectively, comparing our results where possible with experimental and other theoretical data. Finally, in section 5, some conclusions are drawn.

2. Theoretical model and numerical method

The numerical method used for the solution of the time-independent Schrödinger equation is based on a relaxation method for the solution of boundary-value problems [14]. Physically it can be motivated by a continuation of the time-dependent Schrödinger equation on the imaginary time axis. With $\tau = it$ we have

$$-\hbar\frac{\partial\Psi}{\partial\tau} = H\Psi \tag{1}$$

where H denotes the Hamiltonian and Ψ the wave function. In terms of the complete set of eigenfunctions Ψ_n satisfying the time-independent Schrödinger equation

$$H\Psi_n = E_n\Psi_n \tag{2}$$

the general solution of equation (1) is given by

$$\Psi(\tau) = \sum_n c_n e^{-E_n \tau/\hbar} \Psi_n \tag{3}$$

with $c_n = \langle \Psi_n | \Psi(0) \rangle$ being the expansion coefficient of the initial state $\Psi(0)$. Assuming, without loss of generality $E_n > 0$ for all energies, all terms in equation (3) decay with increasing τ; the ground state Ψ_0, however, will have the slowest decay rate, given by $E_0/\hbar$. Thus, except for a normalization constant, the solution of equation (1) approaches the ground state with increasing τ, unless the initial condition is orthogonal with respect to this state. The excited states can be obtained successively by choosing an initial state orthogonal with respect to the already known lower states. Obviously, this technique works only in the case of a discrete spectrum.

After having discussed the general formulation of our procedure, let us now turn to the specific Hamiltonian for the shallow impurity in a multi-quantum-well structure. In the symmetric gauge with the vector potential $\boldsymbol{A} = \frac{1}{2} B \rho \boldsymbol{e}_\phi$ for a magnetic field $\boldsymbol{B}$ perpendicular to the wells, the Hamiltonian is given in cylindrical coordinates (ρ, ϕ, z) according to

$$H = -\frac{\hbar^2}{2m^*} \left\{ \frac{1}{\rho} \frac{\partial}{\partial \rho} \left(\rho \frac{\partial}{\partial \rho} \right) + \frac{1}{\rho^2} \frac{\partial^2}{\partial \phi^2} + \frac{\partial^2}{\partial z^2} \right\} + \frac{e\hbar B}{2m^* \mathrm{i}} \frac{\partial}{\partial \phi} + \frac{e^2 B^2}{8m^*} \rho^2 - \frac{e^2}{4\pi\epsilon\epsilon_0} \frac{1}{\sqrt{\rho^2 + (z - z_I)^2}} + V_w(z). \tag{4}$$

Here, $V_w(z)$ is the quantum-well potential, z_I is the z-coordinate of the impurity, and a single isotropic effective mass m^* has been assumed for the well and for the barrier regions. Due to the cylindrical symmetry of the problem, the z-component of the angular momentum commutes with the Hamiltonian and the eigenfunctions are given by

$$\Psi(\rho, \phi, z) = \psi(\rho, z) e^{\mathrm{i}m\phi} \tag{5}$$

and we end up with a two-dimensional Schrödinger equation for $\psi(\rho, z)$. The corresponding Hamiltonian is obtained from equation (4) by substituting $(\mathrm{i}m)$ for $\partial/\partial\phi$.

To obtain a solution of the problem, the boundary conditions for the wave functions have to be specified. Since we are interested in bound states, the wave function must vanish at infinity (that is for $\rho \to \infty$ and $z \to \pm\infty$). Furthermore, the solution has to be finite everywhere and the first derivative has to be continuous except at the position of the impurity. This leads us to the boundary conditions for $\rho = 0$: (i) For $m \neq 0$, the wave function must vanish at $\rho = 0$ in order to be unique when performing the limit $\rho \to 0$ at different angles ϕ. (ii) For $m = 0$ and $z \neq z_I$ the boundary condition is $\partial\psi/\partial\rho = 0$ in order to have a continous derivative. (iii) The only remaining condition for $m = 0$ and $z = z_I$ is obtained by transforming the Schrödinger equation into spherical coordinates and integrating over a small sphere with radius R around the impurity. When performing the limit $R \to 0$ this results in

$$\int_0^\pi \sin(\theta) \left(\frac{\partial \psi}{\partial r} \right)_{r \to 0} \mathrm{d}\theta = -\frac{m^* e^2}{2\pi\epsilon\epsilon_0 \hbar^2} \psi(0) \tag{6}$$

with $r = \sqrt{\rho^2 + z^2}$ and $\theta = \mathrm{tg}^{-1}(\rho/z)$.

The parabolic differential equation (1) is now solved numerically by using an explicit finite difference scheme with step sizes $\Delta\rho$, Δz, and $\Delta\tau$. After each time step the

wave function $\psi(\rho, z)$ is normalized to a maximum value of unity. The energy $E(\tau) = \langle\Psi|H|\Psi\rangle/\langle\Psi|\Psi\rangle$ is calculated and the result is accepted if $E(\tau - \Delta\tau) - E(\tau) < \Delta E_{\min}$ is reached, where, typically, $\Delta E_{\min} = 5 \times 10^{-4}$ meV. The procedure has been tested by examining the three-dimensional as well as the two-dimensional limit where, in the absence of a magnetic field, the exact energies are known. In these cases, the error in the ground state energy is of the order of 1%. After the calculation of the ground state, a new initial state orthogonal with respect to the ground state is taken and the procedure is repeated. Due to numerical uncertainties, the solution does not remain exactly orthogonal and, therefore, after typically 100 time steps an orthogonalization procedure is performed. In the same way, the excited states E_n are calculated successively up to the desired number $n_{\max}$ by orthogonalization with respect to all lower-lying states.

From equation (3) it is clear that the total time τ needed for a convergence of the nth eigenstate is of the order of several $\hbar(E_{n+1} - E_n)^{-1}$. On the other hand, the convergence of an explicit finite difference scheme poses an upper limit for the time step $\Delta\tau$ of the order of $\Delta\tau < m^*(\Delta z^2 + \Delta\rho^2)/\hbar$. Thus, when increasing the spatial resolution by a factor f the total number of time steps required for convergence increases quadratically in f and consequently the computer time increases by the fourth power in f. This can be avoided by using a multigrid technique [14]. We start with relatively large values of $\Delta\rho$, Δz, and $\Delta\tau$ and solve the equation until the energy converges. The spatial step sizes are now divided by two and the time step is divided by four. Again the equation is solved until convergence is reached. This procedure is repeated up to the desired spatial accuracy. We typically start on a lattice with about 12×16 points and end up on a lattice with 192×256 points.

The parameters chosen in the numerical calculations are the same as those in [9] and [13] corresponding to experiments described in [15], except for the barrier thickness for which different values have been taken. In the next section, we present results for an SQW system where the impurity is placed either in the well or in the barrier. Due to the long range of the Coulomb potential, bound states are observed even for quite large distances of the impurity from the well. In section 4 we present results for an MQW system. We demonstrate that for the barrier width studied in [9], [13] and [15] no coupling between the wells is detectable and we obtain a series of eigenstates localized in the well where the impurity is located, a series of states localized in the neighbouring wells and a series localized in the next-nearest neighbouring wells. When reducing the barrier width these states couple and the full multi-quantum well problem has to be solved.

3. Results for a single-quantum-well system

Calculations have been performed for the case of a 15 nm GaAs quantum well surrounded by $Ga_{1-x}Al_xAs$ barriers with $x = 0.33$ up to a magnetic field of 8 T. For each magnetic quantum number $m = 0, 1, 2, 3$, the four lowest states have been calculated. The energies of the states with negative quantum number m are obtained by simply subtracting the Zeeman energy according to

$$E_{-m} = E_m - \frac{e\hbar B}{m^*}m. \tag{7}$$

The relaxation to an eigenstate is illustrated in figure 1 for the case of $B = 4$ T, $m = 1$ and an impurity in the centre of the well, where the wave function $\psi(\rho, z)$ is plotted at four different values of the imaginary time τ. Figure 1(a) shows the initial state chosen in the calculations. At $\tau = 5$ fs (figure 1(b)) the wave function is already mainly confined

in the well but the impurity has not yet influenced the radial shape. This fast relaxation in the z-direction can be easily understood from equation (3): in order to reproduce a wave function that has a large amplitude in the barrier regions we need eigenstates with the same behaviour. These eigenstates have high energies of the order of the barrier height (253 meV) and, therefore, their contribution decays rapidly. The subsequent build-up of the localization in the radial direction is governed by the energy difference between the bound impurity states and the free states (of the order of 10 meV) and occurs on a slower time scale. At $\tau = 70$ fs (figure 1(c)) this build-up is clearly visible and at $\tau = 500$ fs (figure 1(d)) the calculation has converged towards the lowest eigenstate.

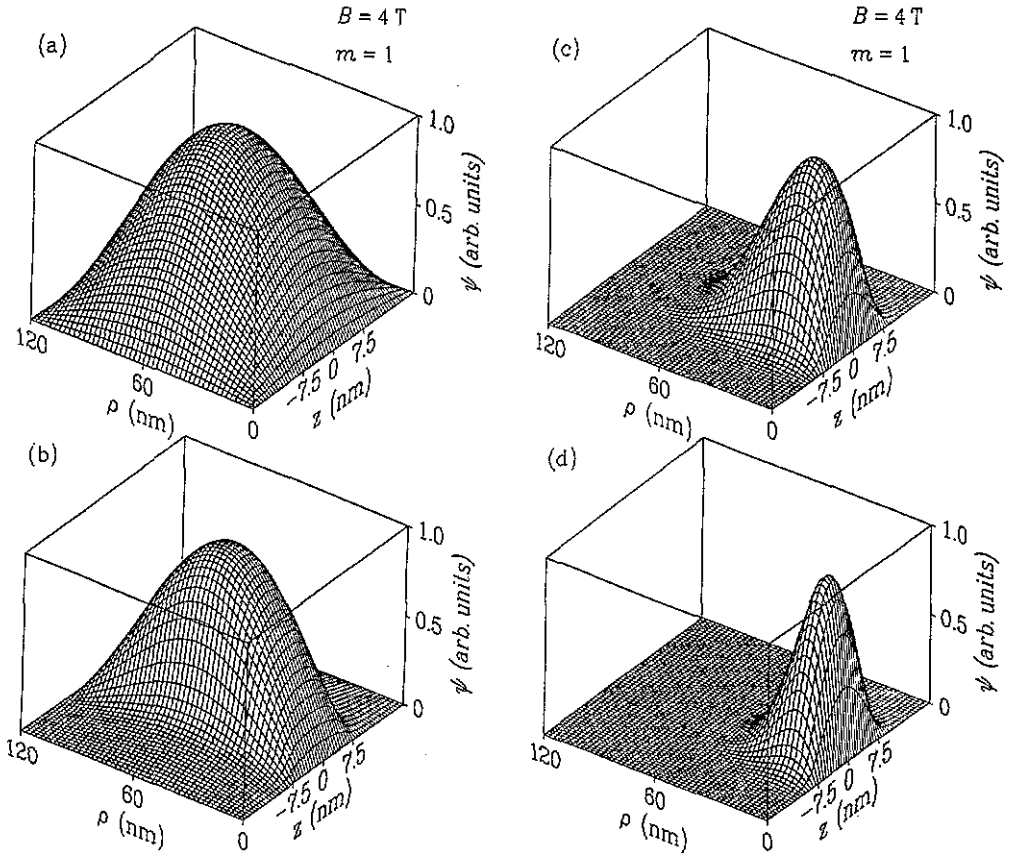

Figure 1. Wave function for the case of $B = 4$ T, $m = 1$ and an impurity in the centre of the well at four different values of the imaginary time τ. (a) $\tau = 0$, (b) $\tau = 5$ fs, (c) $\tau = 70$ fs, (d) $\tau = 500$ fs.

The energies for the case of an impurity placed in the centre of the well are shown in figure 2. With increasing magnetic field we observe the formation of Landau-like states where each Landau level N with $N = 0, 1, 2, \ldots$ has contributions with $m \leqslant N$, as is well known from the theory of two-dimensional systems in a magnetic field [10]. This grouping for a particular N is clearly shown in figure 2. The degeneracy of all these contributions, which is present in the absence of an impurity, is removed by the Coulomb term. The ground state remains well separated from all other states.

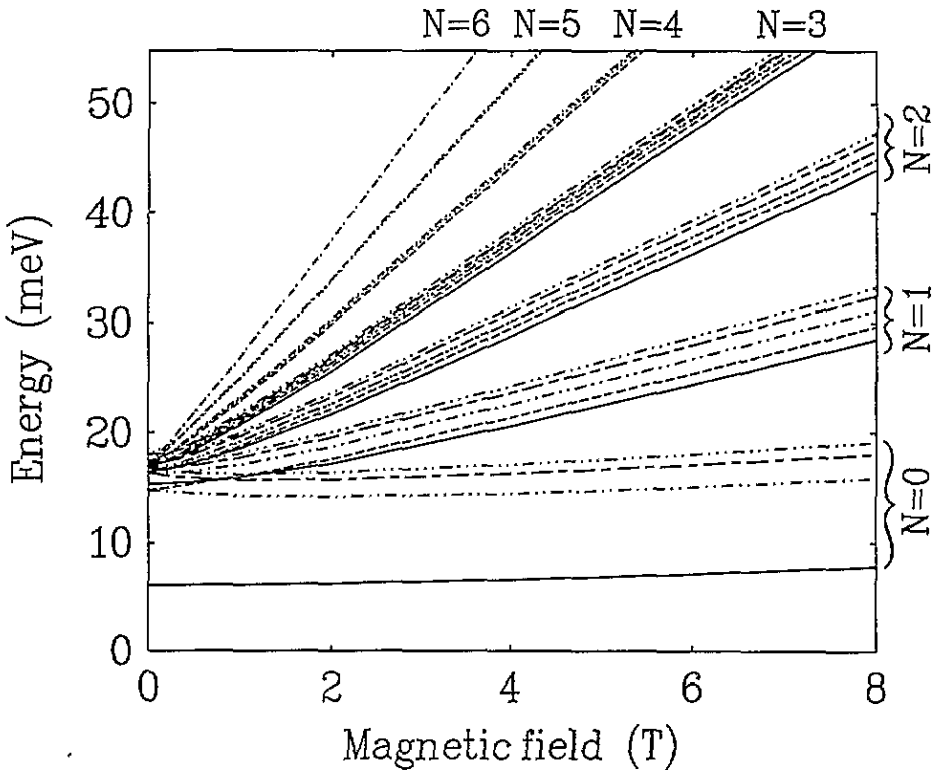

Figure 2. Energy eigenvalues of a hydrogenic impurity in a 15 nm quantum well as a function of the magnetic field. Each line refers to a different magnetic quantum number m: ——, $m = 0$; - - - -, $m = 1$; · · · · · ·, $m = 2$; — · —, $m = 3$; — · · —, $m = -1$; — · —, $m = -2$; — · · — · · —, $m = -3$. With increasing field, states with $m \leqslant N$ group into sets corresponding to a Landau quantum number N.

The binding energies with respect to the Landau levels at an intermediate magnetic field of 4 T are plotted in figure 3. We again note that the ground state has a binding energy much larger than all other states. For both cases, $m > 0$ as well as $m < 0$, the binding energies decrease with increasing $|m|$ due to the reduced overlap of the wave function with the impurity potential. For each Landau level index N the binding energy of a state m is larger than that of the corresponding state $-m$ since the latter has fewer nodes in the radial direction. It is clear from these results that it is not possible to obtain meaningful empirical expressions for the binding energies with respect to the corresponding Landau levels as a function of m for a given value of B such as those quoted in [16].

In an infrared photoconductivity experiment transitions between different impurity levels are measured. Therefore in figure 4 the transition energies from the ground state to the various excited states are shown for the same case as in figure 2. Two series of experimental results [7, 15] have also been included, which correspond to a nominal well width of 15 nm. We find good agreement except for some experimental points just in between two Landau levels. We note subsequently that the widths of the wells in the sample used in the experiments described in [15] were found to be 17.8 nm instead of 15 nm [17], which is the figure quoted and used previously in the above calculations [9]. This error is sufficient to account for the slight discrepancies between our calculations and experiment.

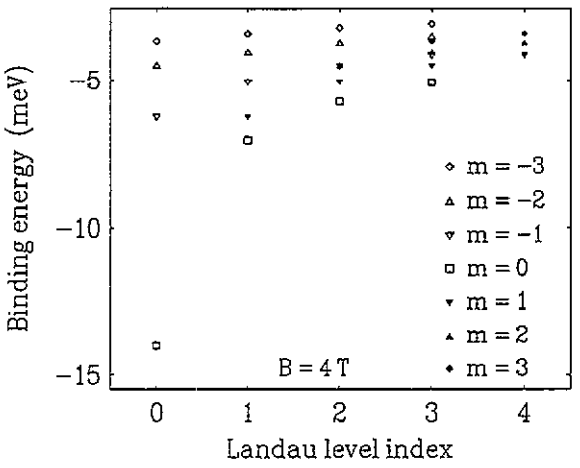

Figure 3. Binding energy of the hydrogenic impurity states with respect to the corresponding Landau level in a 15 nm quantum well at a magnetic field of 4 T.

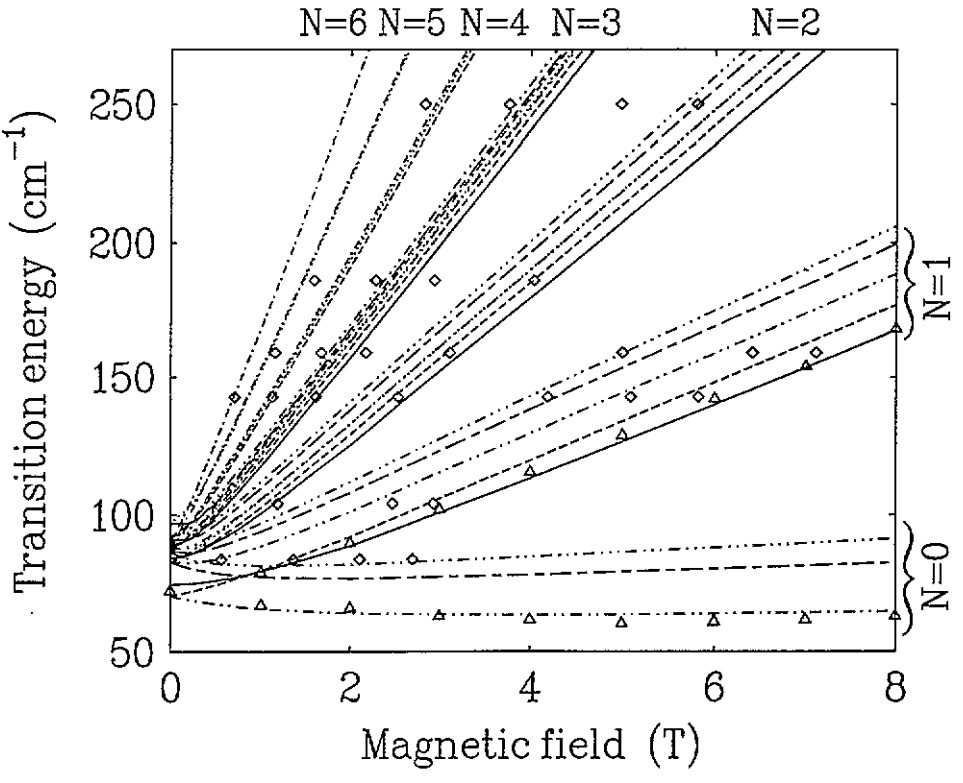

Figure 4. Transition energies between the ground state and excited states. The lines of given m are specified as in figure 2. Symbols refer to experimental results: ◇, [15], △, [7].

Also, taking into account different effective masses in the well and the barriers, as well as different dielectric constants, might also slightly modify the results, but these effects are small. We note also that, on comparing the above calculations of transition energies with those obtained by the matrix diagonalization procedure [9] and the alternative method described in [13], very close agreement is obtained.

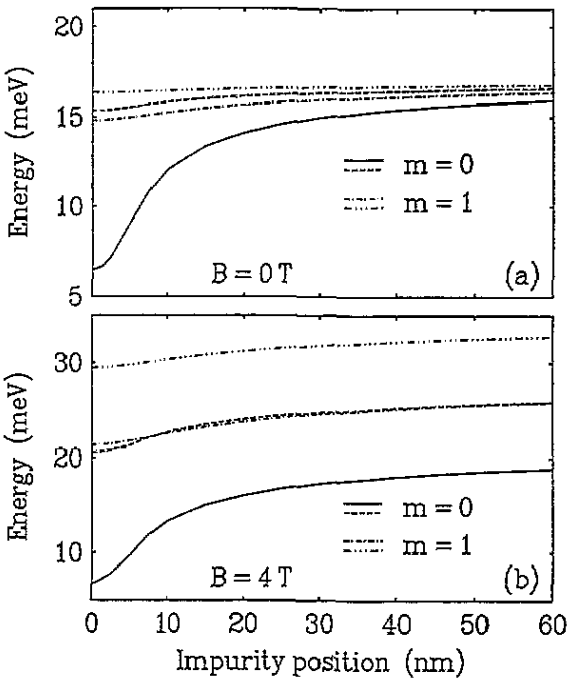

Figure 5. Energy eigenvalues of hydrogenic impurity states in a 15 nm quantum well as function of the position of the impurity, measured from the centre of the well.

An impurity located in the centre of the well produces the largest binding energy. With increasing distance from the centre, the binding energy decreases. Due to the long range nature of the Coulomb potential, however, bound states are still possible even if the impurity is located in the barrier quite far away from the well. This is shown in figure 5 where for the cases of zero magnetic field and a field of 4 T the lowest two states with $m = 0$ and $m = 1$, respectively, are plotted as a function of the impurity position z_1, measured from the centre of the well. Note that for $z_1 > 7.5$ nm the impurity is located in the barrier ('remote impurity'). Even at a distance of 60 nm bound states still exist. In the case of an applied magnetic field, the energies of states with different values of m corresponding to the same Landau level become degenerate as soon as the length scale for a variation of the Coulomb potential inside the well becomes larger than the cyclotron radius.

4. Results for a multi-quantum-well system

Most experiments are performed on MQW systems rather than on SQW systems. One main reason is the increase in sensitivity. Then, however, the fundamental problem arises as

to whether the system simply behaves as an ensemble of SQW systems so that the results shown in the previous section remain valid, or whether the coupling between the wells has to be taken into account. In order to study the role of this coupling, we have performed calculations for the case of five quantum wells of 15 nm width, each separated by identical barriers with varying thickness. The impurity has been placed in the centre of the central well. In this case, due to the symmetry of the problem, the states can be classified according to their z-parity as even ($\psi(\rho, z) = \psi(\rho, -z)$) or odd ($\psi(\rho, z) = -\psi(\rho, -z)$) states.

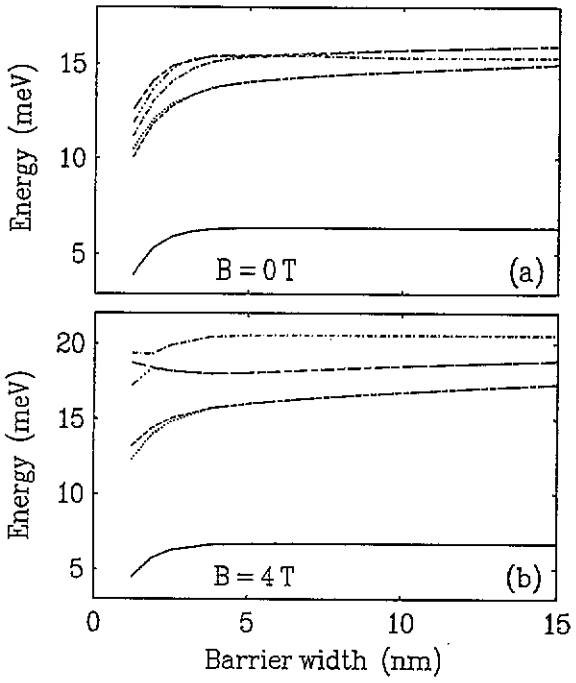

Figure 6. Lowest six energy eigenvalues of hydrogenic impurity states in an MQW system consisting of five 15 nm QWs as a function of the width of the barriers between the wells. The impurity has been placed in the centre of the central well. The dotted and the long–short dashed lines refer to states with odd z-parity, all other lines to states with even z-parity.

The resulting six lowest-energy eigenvalues with $m = 0$ are plotted in figure 6 as a function of the barrier width for two values of the magnetic field. The dotted lines and the long–short dashed lines refer to an odd z-parity, all others to an even z-parity. In the limit of thick barriers we observe two different types of behaviour: two states are independent of the width, while the energy of the other states increases with increasing width. The reason is that the former two states are localized in the central well that contains the impurity, and thus they are not influenced by the presence of other wells. (The energies agree with the values for $z_I = 0$ as shown in figure 5.) When classified according to the high-field notation (N, m, ν), where ν denotes the number of nodes in the z-direction, as is done in [9, 13], these two states refer to $(0, 0, 0)$ and $(1, 0, 0)$.

The other states are localized in wells other than the central one. Their energies agree with the ground state values of figure 5 for $z_I = L_W + L_B$ and $z_I = 2(L_W + L_B)$, respectively, where L_W is the well width and L_B the barrier width. Odd and even z-parity states are

exactly degenerate, which means also that localized states in the left and the right wells are possible eigenstates, and the MQW system behaves like uncoupled SQW systems, each having a different location of the impurity. For these states it is not important that the impurity is located in a quantum well as they behave exactly as if the impurity were in the barrier at the given distance from the well where the state is localized. Thus we may refer to these states as bound states of a 'remote impurity'. In the high-field notation the even states refer to (0, 0, 2) and (0, 0, 4), while the odd states refer to (0, 0, 1) and (0, 0, 3). For small barrier widths the degeneracy is removed and the full MQW sytem has to be taken into account. This is shown clearly by looking at the localization of the states.

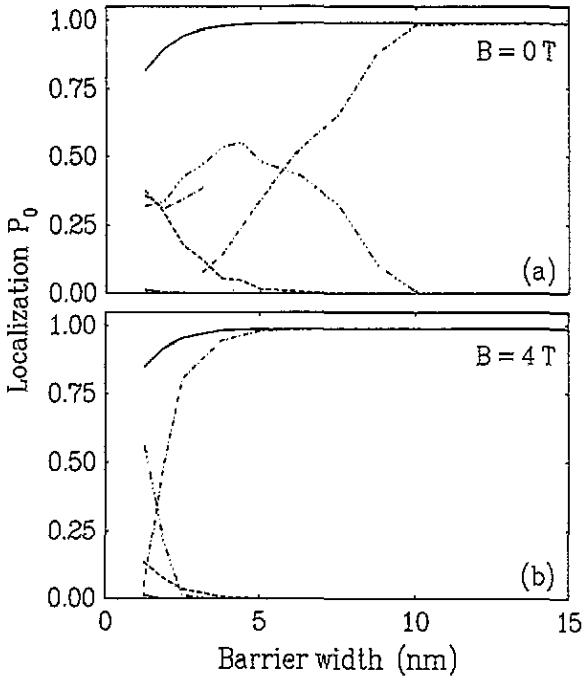

Figure 7. Relative degree P_0 of localization in the central well, (see equation (8)) of the states shown in figure 6. Due to a level crossing with a higher excited state at a barrier width of 3.5 nm, the dash-dotted line in (a) refers to different states below and above this value.

In figure 7 the relative localization in the central well P_0, defined according to

$$P_0 = \int_{-L_W/2}^{L_W/2} dz \int_0^\infty \rho \, d\rho |\psi(\rho, z)|^2 \Big/ \int_{-\infty}^{\infty} dz \int_0^\infty \rho \, d\rho |\psi(\rho, z)|^2 \tag{8}$$

is plotted as a function of the barrier width for the same cases as in figure 6. The odd z-parity states always have a negligible contribution in the central well. In the absence of a magnetic field, for a barrier width above 10 nm the two states with barrier-width independent energies are indeed perfectly localized in the central well, while the other two even z-parity states have no contribution there. With decreasing barrier width, the ground state (solid line) and the first excited state (dashed line) remain localized inside and outside the central well, respectively, while the other states interact with each other due to their

small energy difference, leading to a delocalization over more than one well. From the localization behaviour it turns out that in the case $B = 0$ the dash-dotted line does not refer to the same state when varying the barrier width. In fact, at a barrier width of 3.5 nm there is a crossing with the next higher state not shown in the figures. Thus, below and above this value the curves refer to different states. For very small barrier widths all even z-parity states finally become delocalized due to strong tunnelling between the wells. In the case of an applied magnetic field the energies are more separated so that the states remain localized down to barrier widths below 5 nm.

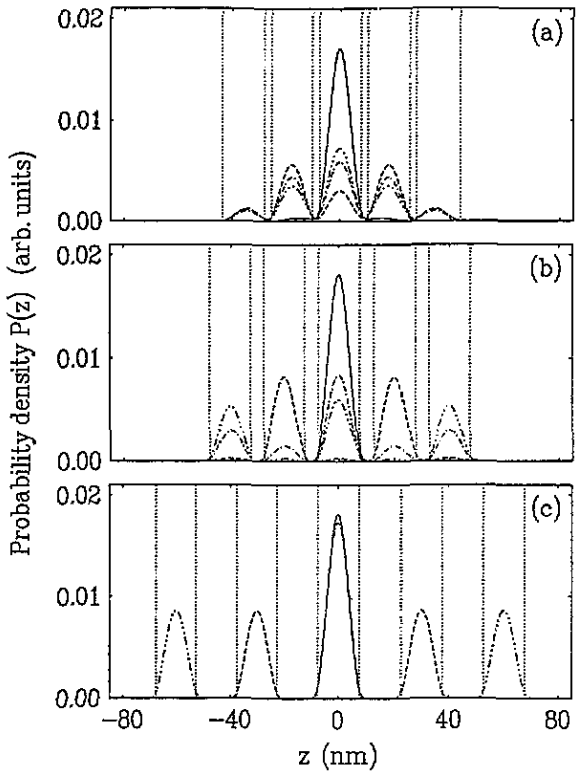

Figure 8. Radially integrated probability density $P(z)$ (see equation (9)) of the states with even z-parity at zero magnetic field for barrier width (a) 2.5 nm, (b) 5 nm, and (c) 15 nm. The lines refer to the four even z-parity energies shown in figure 6. The vertical dotted lines indicate the boundaries between wells and barriers.

The details of this localization are made evident by looking at the radially integrated probability density

$$P(z) = \int_0^\infty \rho \, \mathrm{d}\rho |\psi(\rho, z)|^2 \Big/ \int_{-\infty}^{\infty} \mathrm{d}z \int_0^\infty \rho \, \mathrm{d}\rho |\psi(\rho, z)|^2. \tag{9}$$

For zero magnetic field (figure 8) and for a field of 4 T (figure 9) $P(z)$ is shown for the even z-parity states. Parts (a), (b), and (c) refer to barrier widths of 2.5 nm, 5 nm, and 15 nm, respectively. The boundaries between wells and barriers have been indicated by

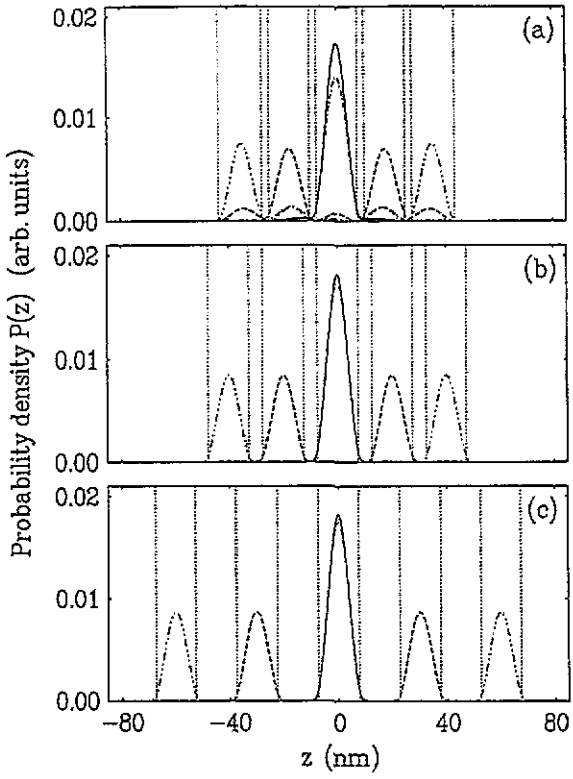

Figure 9. Same as in figure 8, but for a magnetic field of 4 T.

dotted lines. For 15 nm barriers, the value of the experiments in [15], we find two states localized in the central well, one state localized in the nearest neighbour wells and one state localized in the next-nearest neighbour wells. For 5 nm barriers with magnetic field, the localization behaviour is still the same, while without magnetic field we now have two delocalized states. For 2.5 nm barriers all states except for the ground state have noticeable contributions in several wells.

The localization found here for the case of 15 nm barriers is much stronger than that found in previous variational [5] and matrix-diagonalisation [9] calculations. The reason is that in the latter calculations [5, 9] only the lowest state in the lowest miniband of the multi-quantum-well has been included in the basis set of the trial wave function. This state is delocalized over the whole structure. The binding energy of the impurity, however, is much larger than the miniband width (which is negligible for the present case), so that an *ansatz* with only one of the quasi-degenerate miniband states is not justified for the calculation of the localization. On the other hand, for thin barriers the miniband width becomes larger and the delocalized basis is a valid approximation. The present approach does not use such an *ansatz*. It converges automatically towards the state with the correct localization, independent of the barrier width.

5. Conclusions

We have presented a detailed investigation of hydrogenic impurity states in a multi-quantum-

well system under an applied magnetic field. By performing a direct numerical integration of an imaginary-time Schrödinger equation we avoid an expansion of the states in terms of some finite basis set and thus also problems arising in intermediate regions (e.g. between the high-field and the low-field limit or for intermediate barrier widths). For the case of a single-quantum well system, we have analysed the dependence of the binding energies on the impurity position. Due to the long-range nature of the Coulomb potential, bound states exist even for large distances of the impurity from the well. The transition energies between the ground state and excited states show good agreement with experimental results. The comparisons have been limited to wells of width 15 nm because these widths appear more often in the literature but other well widths could have been used.

For the case of an MQW system, we have investigated the dependence of the binding energies and of the localization of the wave functions on the barrier widths. It turned out that for barrier widths above about 10 nm the wave functions are completely localized either within one well or in the two, equivalent (for symmetry reasons) wells. Thus, the use of an SQW system for the analysis of experiments performed on an MQW system with a barrier width of 15 nm is justified. In other methods, which are based on delocalized states for the MQW system, the *full* miniband has to be taken into account if, for increasing barrier width, the miniband width becomes of the order of the binding energy.

Finally, we emphasize that this novel method of calculating the transition energies of impurities in QW systems gives not only accurate results but also important information on the underlying physics associated with the effects of confinement. It shows clearly when an MQW system can be satisfactorily modelled in terms of a sum of SQWs. This method also gives solutions that include both the hydrogen-like functions and metastable states [12, 13] simultaneously, unlike the variational methods, which generally cover the hydrogen-like solutions only [8]. The calculations could form a basis for further calculations modelling real physical systems in which electric fields are applied [1, 2] and the tilting of the magnetic field [17] and for refinements in which the resonant and non-resonant polaron corrections can be incorporated.

Acknowledgments

This work has been partially supported by the Deutscher Akademischer Austauschdienst and the British Council in the establishment of a collaborative research programme between the two laboratories.

References

[1] Barmby P W, Fromhold T M, Dunn J L, Bates C A, Sheard F W and Eaves L 1993 *Mater. Sci. Forum* at press
[2] Sakai J W, Fromhold T M, Beton P H, Henini M, Eaves L, Mason P C, Sheard F W and Hill G 1993 *Physica* B **184** 241
[3] Greene R L and Bajaj K K 1985 *Phys. Rev.* B **31** 913
[4] Greene R L and Lane P 1986 *Phys. Rev.* B **34** 8639
[5] Lane P and Greene R L 1986 *Phys. Rev.* B **33** 5871
[6] Chang Y-H, McCombe B D, Mercy J-M, Reeder A A, Ralston J and Wicks G A 1988 *Phys. Rev. Lett.* **61** 1408
[7] Cheng J-P and McCombe B D 1990 *Phys. Rev.* B **42** 7626
[8] Shi J M, Peeters F M and Devreese J T 1993 *Phys. Rev.* B **48** 5202
[9] Dunn J L and Pearl E 1991 *J. Phys.: Condens. Matter* **3** 8605

[10] MacDonald A H and Ritchie D S 1986 *Phys. Rev.* B **33** 8336
[11] Wagner H P and Prettl W 1988 *Solid State Commun.* **66** 367
[12] van Klarenbosch A, Klaassen T O, Wenckebach W Th and Foxon C T 1990 *J. Appl. Phys.* **67** 6323
[13] Pearl E P, Dunn J L and Bates C A 1992 *J. Phys.: Condens. Matter* **4** L199
[14] Press W H, Teukolsky S A, Vetterling W T and Flannery B P 1992 *Numerical Recipes in FORTRAN* 2nd edn (Cambridge: Cambridge University Press)
[15] Grimes R T, Stanaway M B, Chamberlain J M, Dunn J L, Henini M, Hughes O H and Gills G 1990 *Semicond. Sci. Technol.* **5** 305
[16] Simola J and Virtamo J 1978 *J. Phys. B: At. Mol. Phys.* **11** 3309
[17] Barmby P W, Bates C A, Dunn J L, Grimes R T and Chamberlain J M 1993 *Semicond. Sci. Technol.* **8** 1711